Silver-based surface plasmon waveguide for terahertz quantum cascade lasers

Y. J. Han,* L. H. Li, J. Zhu, A. Valavanis, J. R. Freeman, L. Chen, M. Rosamond, P. Dean, A. G. Davies and E. H. Linfield

School of Electronic and Electrical Engineering, University of Leeds, Leeds LS2 9JT, UK y.han@leeds.ac.uk

Abstract: Terahertz-frequency quantum cascade lasers (THz QCLs) based on ridge waveguides incorporating silver waveguide layers have been investigated theoretically and experimentally, and compared with traditional gold-based devices. The threshold gain associated with silver-, gold- and copper-based devices, and the effects of titanium adhesion layers and top contact layers, in both surface-plasmon and double-metal waveguide geometries have been analysed. Our simulations show that silver-based waveguides yield lower losses for THz QCLs across all practical operating temperatures and frequencies. Experimentally, QCLs with silver-based surface-plasmon waveguides were found to exhibit higher operating temperatures and higher output powers compared to those with identical but gold-based waveguides. Specifically, for a three-well resonant phonon active region with scaled oscillator strength of 0.43 and doping density of 6.83 x 10^{15} cm^{-3}, an increase of 5 K in the maximum operating temperature and 40% increase in the output power were demonstrated. These effects were found to be dependent on the active region design, and greater improvements were observed for QCLs with a larger radiative diagonality. Our results indicate that silver-based waveguide structures could potentially enable THz QCLs to operate at high temperatures.

OCIS codes: (140.5965) Semiconductor lasers, quantum cascade; (140.3070) Infrared and far-infrared lasers.

References and links

1. P. Berini and I. De Leon, "Surface plasmon-polariton amplifiers and lasers," Nat. Photon. 6, 16-24 (2012).
2. J. A. Dionne, L. A. Sweatlock, H. A. Atwater, and A. Polman, "Planar metal plasmon waveguides: frequency-dependent dispersion, propagation, localization, and loss beyond the free electron model," Phys. Rev. B 72, 075405 (2005).
3. C. Sirtori, C. Gmachl, F. Capasso, J. Faist, D. L. Sivco, A. L. Hutchinson, and A. Y. Cho, "Long-wavelength (8-1.5 μm) semiconductor lasers with waveguides based on surface plasmons," Opt. Lett. 23, 1366-1368 (1998).
4. A. Tredicucci, C. Gmachl, F. Capasso, A. L. Hutchinson, D. L. Sivco, and A. Y. Cho, "Single-mode surface-plasmon laser," Appl. Phys. Lett. 76, 2164-2166 (2000).
5. R. Kohler, A. Tredicucci, F. Beltram, H. E. Beere, E. H. Linfield, A. G. Davies, D. A. Ritchie, R. C. Iotti, and F. Rossi, "Terahertz semiconductor-heterostructure laser," Nature 417, 156-159 (2002).
6. B. S. Williams, S. Kumar, H. Callebaut, Q. Hu, and J. L. Reno, "Terahertz quantum-cascade laser at lambda approximate to 100 um using metal waveguide for mode confinement," Appl. Phys. Lett. 83, 2124-2126 (2003).
7. J. R. Gao, J. N. Hovenier, Z. Q. Yang, J. J. Baselmans, A. Baryshev, M. Hajenius, T. M. Klapwijk, A. J. Adam, T. O. Klaassen, B. S. Williams, S. Kumar, Q. Hu, and J. L. Reno, "Terahertz heterodyne receiver based on a quantum cascade laser and a superconducting bolometer," Appl. Phys. Lett. 86, 244104 (2005).
8. J. L. Kloosterman, D. J. Hayton, Y. Ren, T. Y. Kao, J. N. Hovenier, J. R. Gao, T. M. Klapwijk, Q. Hu, C. K. Walker, and J. L. Reno, "Hot electron bolometer heterodyne receiver with a 4.7-THz quantum cascade laser as a local oscillator," Appl. Phys. Lett. 102, 011123 (2013).
9. P. Dean, A. Valavanis, J. Keeley, K. Bertling, Y. L. Lim, R. Alhathlool, A. D. Burnett, L. H. Li, S. P. Khanna, D. Indjin, T. Taimre, A. D. Rakic, E. H. Linfield, and A. G. Davies, "Terahertz imaging using quantum cascade lasers - review of systems and applications," J. Phys. D 47, 374008 (2014).
10. B. S. Williams, S. Kumar, Q. Hu, and J. L. Reno, "Operation of terahertz quantum-cascade lasers at 164 K in pulsed mode and at 117 K in continuous-wave mode," Opt. Express 13, 3331-3339 (2005).
11. M. A. Belkin, J. A. Fan, S. Hormoz, F. Capasso, S. P. Khanna, M. Lachab, A. G. Davies, andE. H. Linfield, "Terahertz quantum cascade lasers with copper metal-metal waveguides operating up to 178 K," Opt. Express 16, 3242-3248 (2008).
12. S. Fathololoumi, E. Dupont, S. G. Razavipour, S. R. Laframboise, G. Parent, Z. Wasilewski, H. C. Liu, and D. Y. Ban, "On metal contacts of terahertz quantum cascade lasers with a metal-metal waveguide," Semicond. Sci. Technol. 26, 105021 (2011).
13. C. W. I. Chan, "Towards room-temperature THz QCLs: directions and design," PhD thesis, Chapter 5 (Massachusetts Institute of Technology, Department of Electrical Engineering and Computer Science, 2015).

14. S. Fathololoumi, E. Dupont, C. W. I. Chan, Z. R. Wasilewski, S. R. Laframboise, D. Ban, A. Matyas, C. Jirauschek, Q. Hu, and H. C. Liu, "Terahertz quantum cascade lasers operating up to ~ 200 K with optimized oscillator strength and improved injection tunneling," Opt. Express 20, 3866 (2012).
15. L. Y. Ying, N. Horiuchi-Ikeda, and H. Hirayama, "Ag-metal bonding conditions for low-loss double-metal waveguide for terahertz quantum cascade laser," Jpn. J. Appl. Phys. 47, 7926-7928 (2008).
16. R. A. Matula, "Electrical resistivity of copper, gold, palladium, and silver," J. Phys. Chem. Ref. Data 8, 1147-1298 (1979).
17. Y. S. Touloukian, R. W. Powell, C. Y. Ho, and P. G. Klemens, *Thermophysical Properties of Matter - The TPRC Data Series. Volume 1. Thermal Conductivity - Metallic Elements and Alloys* (1970).
18. J. R. Waldrop, "Schottky barrier height of ideal metal contacts to GaAs," Appl. Phys. Lett. 44, 1002-1004 (1984).
19. S. H. Pan, D. Mo, W. G. Petro, I. Lindau, and W. E. Spicer, "Schottky barrier formation and intermixing of noble metals on GaAs(110)," J. Vac. Sci. Technol. B 1, 593-597 (1983).
20. P. B. Johnson and R. W. Christy, "Optical constants of the noble metals," Phys. Rev. B 6, 4370-4379 (1972).
21. E. D. Palik, *Handbook of Optical Constants of Solids* (Academic, 1985).
22. M. A. Ordal, R. J. Bell, R. W. Alexander, L. L. Long, and M. R. Querry, "Optical properties of fourteen metals in the infrared and far infrared: Al, Co, Cu, Au, Fe, Pb, Mo, Ni, Pd, Pt, Ag, Ti, V, and W," Applied Optics 24, 4493-4499 (1985).
23. R. L. Olmon, B. Slovick, T. W. Johnson, D. Shelton, S.-H. Oh, G. D. Boreman, and M. B. Raschke, "Optical dielectric function of gold," Phys. Rev. B 86, 235147 (2012).
24. H. U. Yang, J. D Archangel, M. L. Sundheimer, E. Tucker, G. D. Boreman, and M. B. Raschke, "Optical dielectric function of silver," Phys. Rev. B 91, 235137 (2015).
25. S. Babar and J. H. Weaver, "Optical constants of Cu, Ag, and Au revisited," Appl. Opt. 54, 477-481 (2015).
26. D. L. Windt, W. C. Cash, M. Scott, P. Arendt, B. Newnam, R. F. Fisher, and A. B. Swartzlander, "Optical constants for thin films of Ti, Zr, Nb, Mo, Ru, Rh, Pd, Ag, Hf, Ta, W, Re, Ir, Os, Pt, and Au from 24 A to 1216 A," Appl. Opt. 27, 246-278 (1988).
27. D. B. Tanner and D. C. Larson, "Electrical resistivity of silver films," Phys. Rev. 166, 652-655 (1968).
28. D. R. Smith and F. R. Fickett, "Low-temperature properties of silver," J. Res. Natl. Inst. Stand. Technol. 100, 119 (1995).
29. M. Walther, D. G. Cooke, C. Sherstan, M. Hajar, M. R. Freeman, and F. A. Hegmann, "Terahertz conductivity of thin gold films at the metal-insulator percolation transition," Phys. Rev. B 76, 125408 (2007).
30. Z. Cheng, L. Liu, S. Xu, M. Lu, and X. Wang, "Temperature dependence of electrical and thermal conduction in single silver nanowire," Sci. Rep. 5, 10718 (2015).
31. C. Y. Ho, R. W. Powell, and P. E. Liley, "Thermal conductivity of the elements: A comprehensive review," Journal of Physical and Chemical Reference Data 3-1, 1-796 (1974).
32. F. R. Fickett, *Electrical Properties of Materials and Their Measurement at Low Temperatures* (U.S. Government Printing Office, 1982).
33. P. Harrison and A. Valavanis, *Quantum Wells, Wires and Dots: Theoretical and Computational Physics of Semiconductor Nanostructures, Fourth Edition* (John Wiley & Sons, Inc., 2016). Chap. 13.
34. Y. J. Han, W. Feng, and J. C. Cao, "Optimization of radiative recombination in terahertz quantum cascade lasers for high temperature operation," J. Appl. Phys. 111, 113111 (2012).
35. H. Callebaut and Q. Hu, "Importance of coherence for electron transport in terahertz quantum cascade lasers," J. Appl. Phys. 98, 104505 (2005).
36. A. Albo and Q. Hu, "Carrier leakage into the continuum in diagonal GaAs/Alo.i5GaAs terahertz quantum cascade lasers," Appl. Phys. Lett. 107, 241101 (2015).
37. M. I. Amanti, G. Scalari, R. Terazzi, M. Fischer, M. Beck, J. Faist, A. Rudra, P. Gallo, and E. Kapon, "Bound-to-continuum terahertz quantum cascade laser with a single-quantum-well phonon extraction/injection stage," New. J. Phys. 11, 125022 (2009).

1. Introduction

Surface plasmons are electromagnetic waves bound at the interface of two materials where the real part of the dielectric constant of each material has the opposite sign [1,2]. The feasibility of exploiting surface plasmon confinement in an optical waveguide has been demonstrated in the quantum cascade laser (QCL), in which a thin metal layer or a highly doped semiconductor

layer is introduced adjacent to the device active region [3,4]. This approach allows a reduction in the waveguide cladding thickness, which is particularly advantageous for terahertz (THz) frequency QCLs since the growth of suitably thick dielectric waveguides is impractical. Indeed, the first THz QCL employed a semi-insulating-substrate-surface-plasmon (SP) waveguide to achieve low waveguide loss, although at the same time this waveguide also resulted in a poor optical mode confinement [5]. To increase the confinement factor, the double metal (DM) waveguide was introduced, with metal layers immediately above and below the active region, and a significant increase in operating temperature was observed [6]. Low loss waveguides are relevant to the performance of THz QCLs at high operating temperatures, and this is desirable for their practical use in applications including local oscillators for astronomic instrumentation [7,8] THz imaging [9]. In order to reduce the waveguide loss further, different waveguide metals have been investigated. Copper (Cu) has advantages over gold (Au) owing to its higher electrical and thermal conductivities [10-13], and the current record lasing temperature for a THz QCL was achieved by using Cu in a DM waveguide configuration [14]. Compared with Au and Cu, silver (Ag) has higher electrical and thermal conductivities at room temperature [15-17], and can form lower Schottky barrier and better interface on n-type GaAs [18,19], which could be beneficial to lower-loss waveguides.

In this work, using one-dimensional transfer matrix simulations, we investigate the effects of waveguide metals, adhesion layers and top contact layers, and show that Ag-based waveguides yield lower losses for THz QCLs across all practical operating temperatures and frequencies than their Au- and Cu-based counterparts, both in SP and DM waveguide geometries. Experimentally, we investigate THz QCLs with Ag-based SP waveguides, and demonstrate higher operating temperatures and greater output powers when compared to identical devices fabricated with Au-based SP waveguides.

2. Dielectric constants of Ag, Au and Cu films

The optical constants of Ag, Au and Cu films are key parameters governing waveguide performance. However, most published values of these constants are either based on bulk materials or do not apply to the THz frequency range [20-26]. Here, the dielectric constants are calculated based on the measured resistivity of Ag, Au and Cu films fabricated using the same process for QCL waveguide layers. The Drude model has been shown to provide a good approximation for the optical response of Ag, Au and Cu in the THz frequency range [22,24], in which the dielectric function is given by

$$s(m) = \text{ei(w)} + \text{is}\,2(m) = 1 \tag{1}$$

where m_p is the plasma frequency,

$$^{m}\text{p} \qquad \frac{ne^2}{ms_0}, \tag{2}$$

is the damping frequency,

$$= \text{-}, \tag{3}$$

n is the electron density, e is the electron charge, m is the effective mass, s_0 is the vacuum dielectric constant, and τ is effective relaxation time. The dc conductivity is given by

$$^{\wedge}0 = \frac{ne^2\tau}{m} \quad \frac{ne^2}{mmd} \tag{4}$$

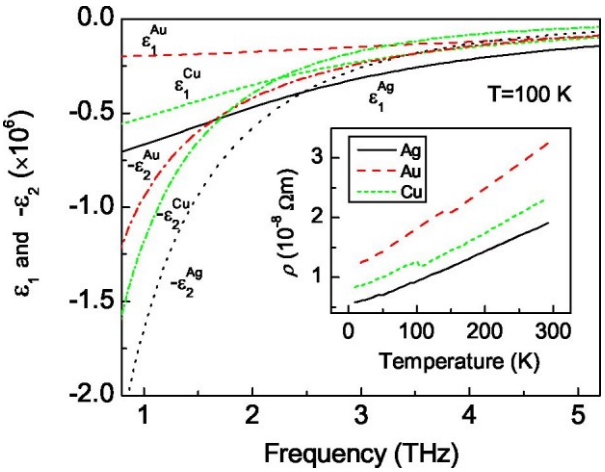

Fig. 1. Calculated dielectric constants of Ag, Au and Cu films at 100 K. The inset shows the temperature evolution of the measured resistivity (p) of the Ag, Au and Cu films.

Assuming that the electron density and the plasma frequency are not affected by sample preparation methods and maintain the same values as those of bulk materials, the damping frequency can therefore be calculated from the conductivity using Eq. (2) and Eq. (4).

Metal films of Ti/Ag (10/200 nm), Ti/Au (10/150 nm) and Ti/Cu (10/200 nm) with dimensions of 2000 x 100 pm^2 were deposited on quartz substrates by electron-beam evaporation, and their resistivities ($p = 1/<r_0$) measured using a four-probe method. As shown in the inset to Fig. 1, the resistivity of the Ag film was found to be 1.91 x10^{-8} Qm at room temperature, which is lower than the respective values of 3.25x10^{-8} Qm and 2.33x10^{-8} Qm obtained for the Au and Cu films. Compared with bulk materials, the films have higher resistivity owing to structural scattering phenomena such as surface scattering and grain boundary scattering [16,27-30]. As the temperature is reduced, the resistivity of both films decreases, and a regression to the Bloch-Gruneisen formula [30] yields a Debye temperature of 202 K, 163 K and 297 K for the Ag, Au and Cu films, respectively, which are close to those for corresponding bulk materials: 221 K, 178 K, and 310 K [31]. Using the plasma frequencies 1.369 x 10^{16} Hz, 1.371 x 10^{16} Hz and 1.123 x 10^{16} Hz [22], and the damping frequencies 1.55 x 10^{13} Hz, 3.03 x 10^{13} Hz and 1.42 x 10^{13} Hz, the dielectric constants of the Ag, Au and Cu films at 100 K can be calculated using Eq. (1). The results are shown in Fig. 1, and reveal larger absolute values of both the real and imaginary parts of the dielectric constant compared to those of Ag, Au and Cu bulk materials. Notably, there are small peaks in resistivity at 45 K and 90 K for Ag, at 145 K for Au, and at 100 K for Cu; these features may be related to impurities [32] but have negligible influence on the waveguide simulations.

3. Waveguide analysis

Waveguide analysis was performed using a one-dimensional transfer matrix solver for THz QCL devices with both SP [5] and DM [6] ridge waveguides. The waveguide structure consists of a 10-pm-thick active region sandwiched between top and bottom waveguide layers. To provide a numerical comparison we assume a 3.1 THz three-well resonant-phonon active region [14], this design is labelled A2 in the experimental section 4, below. The top waveguide layers are same for both SP and DM geometries, and comprise a 50-nm-thick n-GaAs layer with a Si doping concentration of 5 x 10^{18}cm^{-3} and a 150-nm-thick waveguide metal layer. The bottom waveguide layers are: a 700-nm-thick n-GaAs layer with a Si doping concentration of 2 x 10^{18}cm^{-3}, a

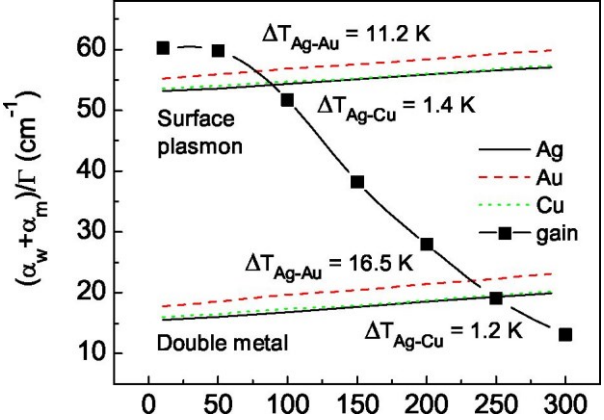

Fig. 2. Temperature evolution of the calculated peak gain (black squares), and the threshold gain for devices with Ag (black solid lines), Au (red dashed lines) and Cu-based (green dots) surface-plasmon waveguides and double metal waveguides. The peak gain is from a 3.1-THz QCL based on a three-well resonant phonon design [14].

$$Sth = \frac{{}^{a}m + {}^{a}w}{\mathrm{r}} \tag{5}$$

20-jum-thick semi-insulating GaAs layer, and a 150-nm-thick waveguide metal layer for the SP waveguide; and a 50-nm-thick n-GaAs layer with a Si doping concentration of 5 x 10^{18}cm^{-3}, and a 1-um-thick waveguide metal layer for the DM waveguide. The calculation of the dielectric constants for GaAs-based QCL materials have been described elsewhere [33]. To compare the Ag, Au and Cu-based waveguides, the threshold gain for each QCL device was calculated as

where a_m is the mirror loss, a_w is the waveguide loss and r is the confinement factor. For a given waveguide configuration (SP or DM), a_m and r are similar for the Ag, Au and Cu-based devices, and so the difference between threshold gain is mainly due to the difference in a_w. The optical peak gain of the 3.1 THz three-well resonant-phonon active region [14] was calculated using a Monte Carlo method [34]; the calculated peak gain and threshold gain at 3.1 THz are plotted in Fig. 2 as a function of temperature. It can be seen that Ag-based waveguides are less lossy than Au and Cu waveguides, and therefore result in lower threshold gain. The results of waveguide loss at 100 K are summarised in Table 1. For the SP waveguide, the waveguide losses are a_w = 13.52 cm^{-1}, 14.39 cm^{-1} and 13.66 cm^{-1} for Ag, Au and Cu-based waveguides, respectively. Considering the corresponding confinement factors of 0.3518, 0.3516 and 0.3518, Ag waveguides yield improvements in threshold gain of 2.51 cm^{-1} and 0.40 cm^{-1} compared with Au and Cu waveguides respectively. For the DM waveguide, the difference of waveguide loss is larger; but owing to the confinement factor of nearly 1.0, Ag waveguides yield threshold gain improvements of 2.82 cm^{-1} and 0.49 cm^{-1} compared with Au and Cu waveguides respectively, which is a little larger than that for the SP waveguide. With increasing temperature, the waveguides become lossier, and at 290 K, the improvement of the threshold gain in the Ag waveguides relative to Au and Cu changes slightly to 2.81 cm^{-1} and 0.26 cm^{-1} for SP waveguides, and 3.16 cm^{-1} and 0.34 cm^{-1} for DM waveguides, respectively. The loss spectrum of each waveguide was also calculated at 100 K. As shown in Fig. 3, Ag-based waveguides yield a lower threshold gain throughout the spectral range from 1 THz to 5 THz. Compared to Cu, the improvement in the threshold gain is around 0.5 cm^{-1} for both SP and DM waveguides. The improvement between Ag and Au is much larger. For the SP waveguides, the maximum improvement in threshold gain is

Table 1. Waveguide analysis results of Ag and Au-based surface-plasmon (SP) and double metal (DM) waveguides at a frequency of 3.1 THz and temperature of 100 K. a_m is the mirror loss, a_w is the waveguide loss, r is the confinement factor, and g_th is the threshold gain. The cavity length of 2000 yum, and the mirror reflectivity of 0.82 for DM waveguides, are used in the calculation.

Waveguide	*am (cm^{-1})*	*a_w (cm^{1})*	r	*gth (cm^{-1})*
Ag - SP	5.60	13.52	0.3518	54.35
Au - SP	5.60	14.39	0.3516	56.86
Cu - SP	5.60	13.66	0.3518	54.75
Ag - DM	0.99	15.87	0.9998	16.87
Au - DM	0.99	18.69	0.9998	19.69
Cu - DM	0.99	16.36	0.9998	17.36

2.50 cm^{-1} obtained at 3.1 THz. In the case of the DM waveguide, the improvement in threshold gain increases from 1.4 cm^{-1} at 1 THz to 3.7 cm^{-1} by 5 THz, which indicates that greater improvements could be expected at even higher frequencies by using Ag-based waveguides.

Lower waveguide loss is expected to result in better device performance. To quantify this improvement, the calculated optical peak gain of the 3.1 THz active region (A2) was compared with the threshold gain for devices with Ag, Au and Cu-based waveguides. As shown in Fig. 2, the maximum operating temperatures are predicted to be 77.6 K and 232.3 K for devices with Au-based SP and DM waveguides, respectively. By replacing Au with Ag, the threshold gain is lowered, and improved operating temperatures of 88.8 K and 248.8 K are predicted for QCLs with identical waveguide configurations. Cu-based waveguides are predicted to be a little lossier than Ag-based ones, but much better than Au-based ones, yielding maximum operating temperatures of 87.4 K and 247.6 K for the devices with SP and DM waveguides respectively. Notably, the increase in predicted operating temperature depends not only on the loss difference between Ag and Au, Cu waveguides, but also on the rate of degradation of the optical gain with increasing temperature; a smaller degradation rate will lead to a larger increase in the maximum operating temperature. The predicted maximum operating temperature for the device with a Au-based DM waveguide is higher than that obtained experimentally [14], which indicates that the degradation rate of the optical gain with temperature was underestimated in our model [35, 36]. In this case, the actual increase in the operating temperature of Ag-based devices might be a little smaller than that predicted above.

The output power is related to the net gain, which is consumed by stimulated emission above threshold. For the three-well resonant phonon design (A2 in the Table 2), we assume that the stimulated emission has a small influence on the carrier injection efficiency to the upper laser level, n, the parasitic scattering lifetime from the upper laser level, τ_{U0}, and the total carrier density in the upper and lower laser levels, $n = n_u + n_l$ .In this case, the stimulated emission lifetime, , can be described using a two-subband system,

where An is the population inversion, τ_U is the lifetime of the higher laser level, *r* is the lifetime

$$An = n\left(\frac{2\,nru\,T_{UQ}}{nrui\;T_{UQ} + (1 - n)Tui\;r + r} \quad 1\right), \tag{6}$$

$$\frac{1}{T_{ul}} \quad \frac{11}{rsr + r^{st}}, \tag{7}$$

$$1 = 1\ 1\ {}^{T}U\ {}^{T}UI \tag{8}$$

$$0$$

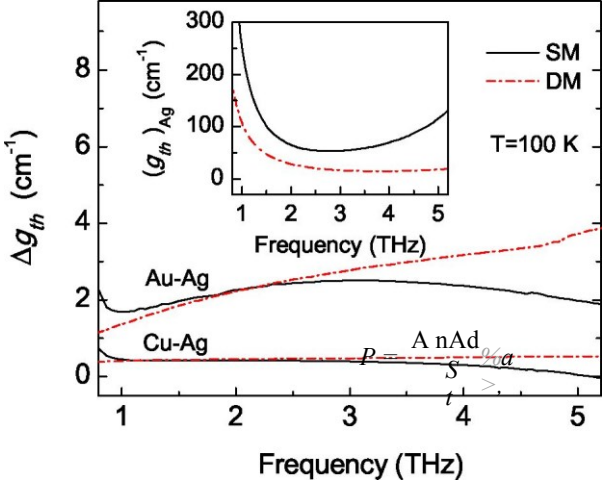

Fig. 3. The difference between the calculated threshold gains for Ag, Cu-based waveguides and Au-based waveguide, plotted as a function of frequency at a temperature of 100 K. SP and DM indicate the surface-plasmon waveguide and the double metal waveguide, respectively. The inset shows the threshold gain for Ag-based waveguides.

$$P = \frac{A\,n\,A\,d}{S} \qquad (9)$$

of the lower laser level, r_{ul} is the scattering lifetime from upper to lower laser level, and τU is the lifetime associated with non-radiative processes. The output power, P, is given by

ul

where A is the area of laser ridge, d is the thickness of active region, is the photon energy, As shown in Fig. 2, the optical gain (g <*x An)* is 60.26 cm^{-1} at 10 K when stimulated emission is not included (τ_{ul} =), corresponding to the values, τ_l = 1.07 ps, τ_{ul} = 10.51 ps, r_{u0} = 12.59 ps, and n = 60.72%, obtained from the Monte-Carlo simulation. For devices with Ag, Au and Cu-based SP waveguides, stimulated emission lowers the optical gain to the threshold values 53.17 cm^{-1},55.22 cm^{-1} and 53.54 cm^{-1}, respectively, and the lifetime of the stimulated emission and the population inversion can be calculated by Eq. (6) and Eq. (7), giving = 30.20 ps, 43.07 ps and 31.94 ps, and An = 0.560n, 0.582n and 0.564n, respectively. Therefore, the output power is estimated to be 37% and 5% higher for the device with a Ag-based SP waveguide, compared to the Au- and Cu-based SP device, respectively. For the DM waveguide, the decrease in the threshold gain is much smaller than the net gain, and the Ag-based waveguide can only yield an increase in output power of 7% and 1% compared to the Au and Cu waveguides, respectively.

The adhesion layer, Ti, deposited between the top contact layer and the waveguide metal films, is not been included in the waveguide analysis above. The conductivity of Ti is much lower than Au, and could introduce more waveguide loss. To investigate the contributions of the adhesion layer, the waveguide analysis was performed for the Ag-based waveguides. The resistivity of a 150 nm Ti film was measured at room temperature as 1.68x 10^{-6} Qm, and the dielectric constants were calculated using the plasma frequency of 3.824x10^{15} Hz [22] and the damping frequency of 2.176x10^{14} Hz. In the waveguides calculations, we assume an abrupt interface between Ti and Ag layers, and the top n+ GaAs layer is removed. As shown in Fig. 4 , with the variation of the thickness of the Ti layer, its effects are dependent on the waveguide configuration. In the case of SP waveguides, the evolution of the threshold gain with respect to the Ti layer thickness is divided into two regions. When the Ti layer is thinner than 50 nm, the threshold gain decreases with increasing Ti thickness, and when the thickness is greater than 50 nm, the threshold gain

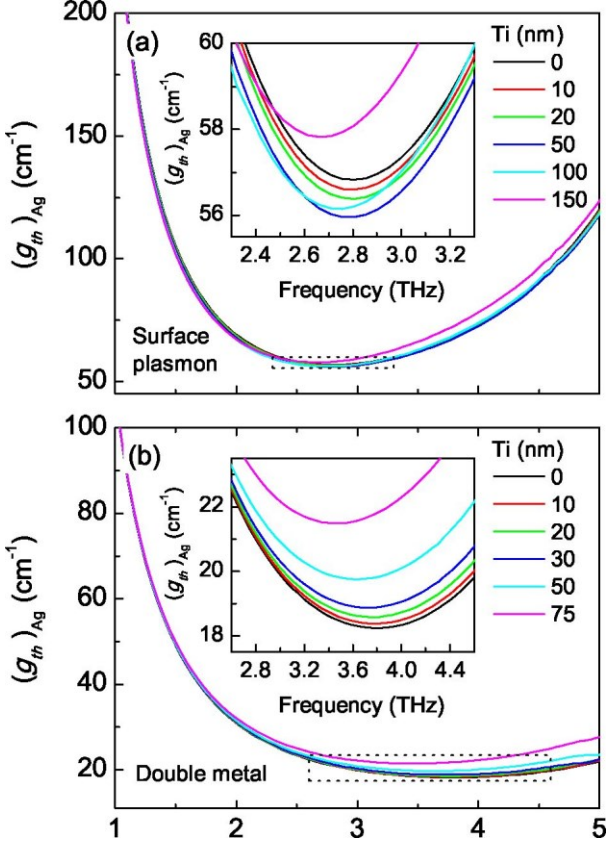

Fig. 4. The room temperature threshold gain as a function of frequency for the Ag-based surface-plasmon waveguide (a) and double metal waveguide (b) with different thickness of Ti adhesion layer. The insets show enlarged figures in the dotted squares.

starts to rise rapidly. The lowest value of the threshold gain is 55.96 cm^{-1} at the Ti layer thickness of 50 nm for the Ag-based SP waveguide, which is 0.87 cm^{-1} lower than that without Ti layer. In the case of the DM waveguide, the threshold gain keeps increasing with the Ti layer varying from 0 nm to 75 nm. At a Ti layer thickness of 10 nm, the lowest threshold gain is 18.38 cm^{-1}, which is 0.14 cm^{-1} higher than that without Ti layer. With increasing Ti layer thickness, the lowest values of threshold gain show a red-shift for both waveguides, from 2.80 THz to 2.66 THz for the SP waveguides, and from 3.82 THz to 3.43 THz for the DM waveguide.

The effects of the top contact n+ GaAs layer were also calculated for the Ag-based waveguides with the Ti layer removed. The loss spectra are shown in Fig. 5 . The top contact GaAs layer has similar effects to the Ti layer. For the SP waveguide, the threshold gain starts with a slow decrease from 56.83 cm^{-1} to 54.50 cm^{-1} with the increase of the top contact layer from 0 nm to 200 nm, and then changes to have an intense increase when the top GaAs layer is thicker. The lowest value of the threshold is shown to occur at 2.80 THz without the top GaAs layer and shift to 2.51 THz at a thickness of 400 nm. In the case of DM waveguides, the top GaAs contact layer results in an increase in waveguide loss. The lowest threshold gain is 18.88 cm^{-1} for a 50 nm GaAs layer, which is 0.53 cm^{-1} higher than the value of 18.25 cm^{-1} obtained for a waveguide without the GaAs layer. The red-shift of the threshold is from 3.82 THz without the top GaAs

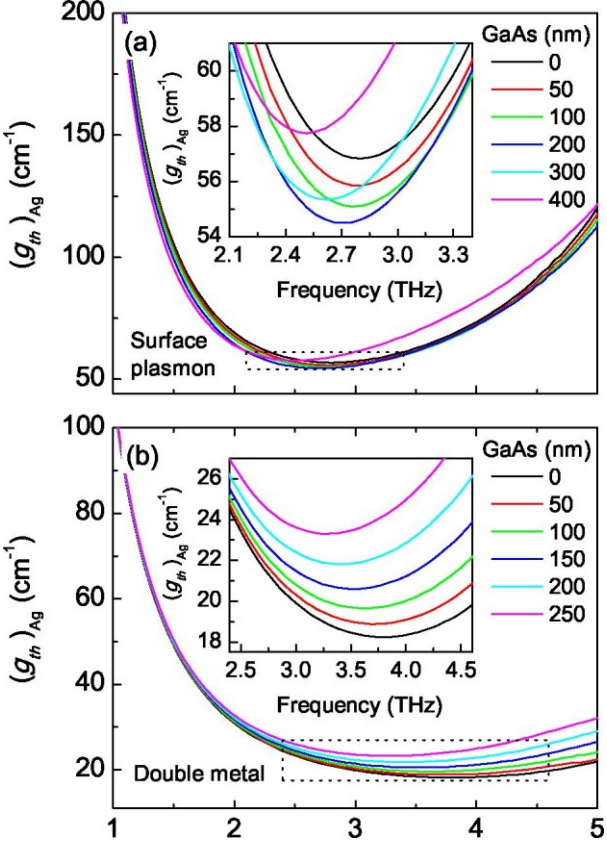

Fig. 5. The room temperature threshold gain plotted as a function of frequency for the Ag-based surface-plasmon waveguide (a) and double metal waveguide (b) with different thickness of GaAs top contact layer. The insets show enlarged figures in the dotted squares.

layer, 250 layer, layer, the GaAs layer other such the layer. to 3.28 THz at a thickness of nm. A thin top GaAs contact as well as a thin adhesion Ti can result in a decrease in threshold gain for SP waveguides, rather than for DM waveguides. This indicates that additional loss from the top contact layer and the adhesion can be compensated by the decrease in the loss from the parts of the SP waveguides, as the bottom n+ GaAs layer, because the distribution of the optical field can be affected by top GaAs layer and the adhesion The normal thicknesses of the adhesion layer and the top GaAs layer are 10 nm and 50 nm respectively, which will contribute to the threshold gain with values less than 0.23 cm^{-1} and 0.96 cm^{-1} for SP waveguides, 0.14 cm^{-1} and 0.64 cm^{-1} for DM waveguides, respectively.

The resistivities of metal films are larger than those of bulk materials, with measured values of 1.91x10^{-8} Qm, 2.33x10^{-8} Qm, 3.25x10^{-8} Qm and 1.68x10^{-6} Qm at room temperature for Ag, Au, Cu, and Ti films, compared to 1.61x10^{-8} Qm, 2.201x10^{-8} Qm, 1.70x10^{-8} Qm and 4.31x10^{-5} Qm for the corresponding bulk materials [22]. Loss spectra were calculated using film and bulk parameters, respectively, for Ag-, Au- and Cu-based waveguides. In the calculation, a 50 nm GaAs top contact layer and a 10 nm Ti layer are included. As shown in Fig. 6, the loss spectra curves are quite similar, and the waveguide losses from using films parameters are larger than those from parameters of bulk materials, in both SP and DM waveguides. However, the

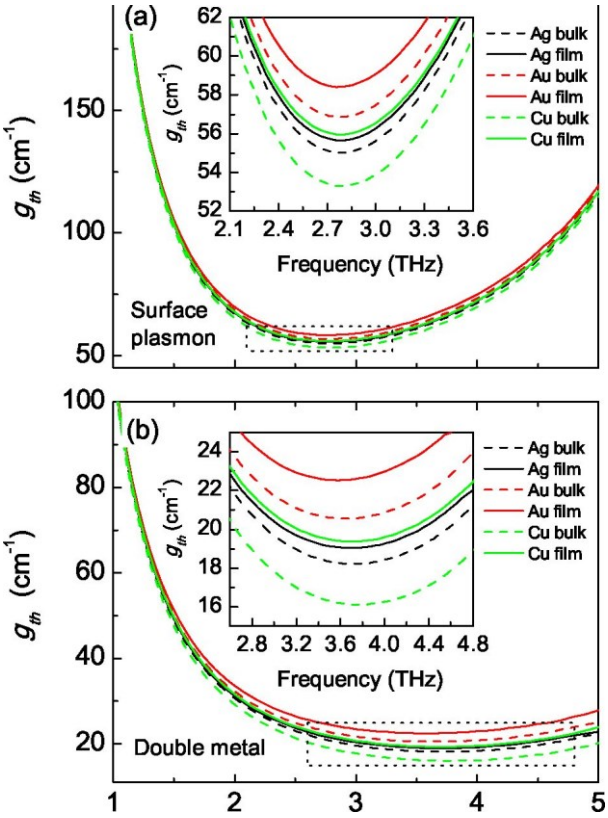

Fig. 6. The room temperature threshold gain as a function of frequency for the Ag, Au and Cu-based surface-plasmon waveguide (a) and double metal waveguide (b). The threshold gains are calculated using the dielectric constants from the metal films and bulk metals, respectively. The insets show enlarged figures in the dotted squares.

Frequency (THz)

increase in the threshold gain is shown to be different, varying from 0.7 cm^{-1} to 3.0 cm^{-1} for the lowest threshold gain. This results in different conclusions about Ag- and Cu-based waveguides. When using the parameters of bulk materials, the best waveguide materials, in decreasing order, are Cu, Ag and Au. Compared to Au-based waveguides, the decrease in the lowest threshold gain is 3.57 cm^{-1} and 1.83 cm^{-1} for Cu- and Ag-based SP waveguides, and the decrease is found to be 4.43 cm^{-1} and 2.32 cm^{-1} for Cu- and Ag-based DM waveguides respectively. When the film parameters are used, the best waveguide materials, in decreasing order, change to Ag, Cu and Au. Compared to Cu and Au, Ag film yields a decrease in the lowest threshold gain of 0.29 cm^{-1} and 2.75 cm^{-1} for SP waveguides, and 0.34 cm^{-1} and 3.49 cm^{-1} for DM waveguides, respectively.

4. QCL characterization results

In this section, we experimentally compare the performance of four THz QCL wafers processed in SP waveguide devices. The samples were grown on semi-insulating GaAs substrates using molecular beam epitaxy. For each wafer, the active region structures were grown to a total thickness of 10 μm and were sandwiched in between n-type GaAs layers. The thickness and the doping concentration of the bottom and top n-type GaAs layers are same as those described in

Table 2. Key parameters of the wafers characterized experimentally. Wafers A1 and A2 are based on a three-well resonant phonon active region [14] with different scaled oscillator strengths (f_{ul}). Wafers B1 and B2 are based on an active region with interlaced bound-to- continuum (B-to-C) and a phonon extraction stages [37] with different doping concentrations and device lengths. Two nominally identical laser ridges were fabricated from each wafer, one is with a Ag-based surface-plasmon (SP) waveguide and the other with a Au-based SP waveguide, giving eight lasers in total in this study.

Wafer	*Active region*	*ful*	*Doping (cm ^{3})*	*Dimensions (pm^2)*
A1	resonant phonon	0.32	6.83 x 10^{15}	1500x150
A2	resonant phonon	0.43	6.83 x 10^{15}	1500x150
*B*1	B-to-C + phonon extraction	0.36	5.61 x 10^{15}	3000x150
B2	B-to-C + phonon extraction	0.36	1.90 x 10^{16}	1500x150

Table 3. Key characterisation results of QCLs with Ag- and Au-based surface-plasmon (SP) waveguides. J_th is the threshold current density at 10 K, P_{max} is the maximum peak output power at 10 K, and T_{max} is the maximum operating temperature.

Wa fer	*SP waveguide*	*J_{th} (kA/cm^2)*	*P_{max} (mW)*	*Tmax (K)*
*A*1	Ag	0.7316	55.0	96
*A*1	Au	0.7324	26.7	83
*A*2	Ag	0.8596	69.3	97
*A*2	Au	0.8643	49.5	92
*B*1	Ag	0.2282	84.8	107
*B*1	Au	0.2320	70.4	102
*B*2	Ag	0.5365	79.0	96
*B*2	Au	0.5614	53.0	95

Section 3. Four wafers labeled A1, A2, B1 and B2 are compared in Table 2. A1 and A2 are based on a three-well resonant-phonon active region design [14], with a larger oscillator strength in the case of A2. B1 and B2 are based on a design with interlaced bound-to-continuum and phonon extraction stages [37], with a higher doping in the active region of B2. Pairs of nominally identical laser ridges with SP waveguides were fabricated from each wafer, giving eight lasers in total. The devices for wafers A1 and B1 were fabricated together except for the metallization stage, while the devices for wafers A2 and B2 were fabricated separately. Ridges were defined by wet chemical etching. AuGeNi layers were deposited to form two 250-pm-wide bottom contacts and two 10-pm-wide top contacts, which were annealed at 400 °C for 1 minute and 270 °C for 4 minutes, respectively. Electron-beam evaporation was employed to deposit waveguide metal layers on the top of each laser ridge and the backside of substrate, using Au for one device in each pair, and Ag for the other. Ti/Ag/Ti/Au (10/200/10/80 nm) layers were used for Ag-based waveguides while Ti/Au (10/150 nm) layers were used for Au-based waveguides. The oscillator strength, doping concentration and device dimensions are listed in Table 2. The devices were mounted on the cold-finger of a helium-cooled Janis ST-100 continuous-flow cryostat and characterized using a Bruker IFS/66 Fourier-transform infrared spectrometer and a QMC Ge:Ga photoconductive detector. The output power was calibrated using a TK Instruments photoacoustic THz absolute power meter.

The temperature evolution of the device performance is compared in Fig. 7 for the Ag- and Au-based devices of each wafer, and the measured data are listed in Table 3. As shown, all the Ag-based devices have a higher maximum lasing temperature, higher output power and

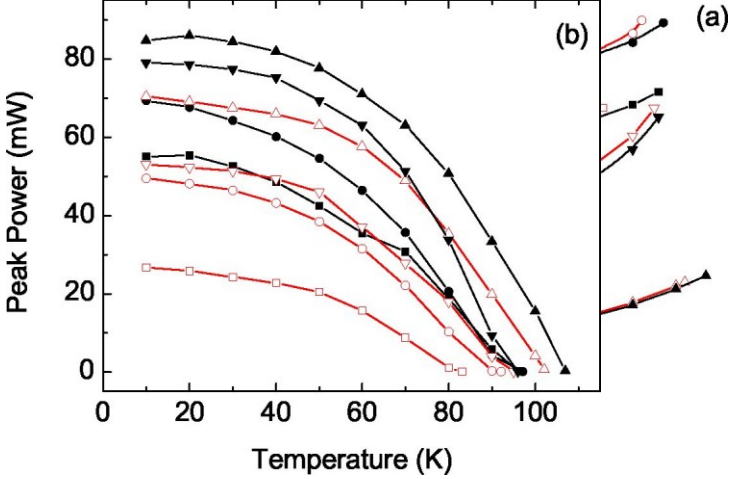

Fig. 7. The threshold current density (a) and peak output power (b) measured from four pairs of QCLs (A1, A2, B1 and B2) as a function of heat-sink temperature. For each pair of devices, the only difference is the waveguide metal layer.

lower threshold current density compared to the equivalent Au-based devices. This indicates that Ag-based waveguides exhibit lower losses than Au-based waveguides, which agrees with the waveguide analysis presented in Section 3. The devices A2 have the same active region structure as that used in the modeling (shown in Fig. 2). Their maximum operating temperatures were determined to be 92 K and 97 K, representing a 5-K increase for the Ag-based device. At a temperature of 10 K, the peak output powers are 49.5 mW and 69.3 mW, respectively, representing a 40% increase for the Ag-based device. The difference between the threshold current density is small, only 4 A/cm^2. The increase in the peak output power between the Ag-based device compared with the Au-based device agrees well with the modeling results, while the increase in the maximum operating temperature is smaller than that predicted (shown in Fig. 2). We attribute this overestimated operating temperature to the small degradation of the calculated peak gain with increasing temperature. If a linear temperature degradation of the gain between 90 K and 200 K is assumed instead, better agreement between the theoretical prediction and experimental data is obtained. In this case 7-K and 10-K increases in the maximum operating temperature are predicted for the devices with Ag-based SP and DM waveguides, respectively.

The performance improvements obtained in Ag-based devices were found to be dependent on the active region design of the THz QCL. The effects of the radiative diagonality and doping

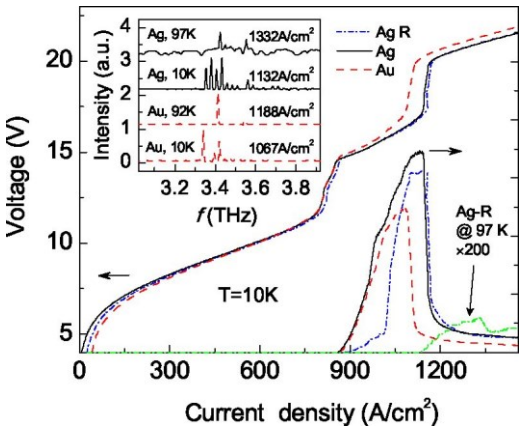

Fig. 8. LIV curves of QCLs (pair A2) with Ag and Au waveguide layers measured at 10 K. The inset shows the emission spectra measured at 10 K and at the maximum operating temperatures. The devices were driven by 2 us-wide current pulses with a duty cycle of 2%. Ag-R indicates the re-characterised LIV curves of the Ag-based device after it had been placed in air for more than two years.

concentration can be investigated via wafers A1 and A2, as well wafers B1 and B2. Compared with the A2 active region, the A1 design has a smaller oscillator strength (see Table 2). This will cause a smaller peak gain and smaller degradation of the gain with temperature, and hence, is expected to provide greater performance improvements when fabricated in a Ag waveguide. Experimentally, the Ag-based A1 device exhibits a 10-K increase in the maximum operating temperature and a 120% increase in the output power compared to the corresponding Au-based device. Comparing the B1 and B2 designs (with doping concentrations 5.61 x 10^{15} cm^{-3} and 1.90 x 10^{16} cm^{-3}, respectively), the higher doping in B2 leads to greater degradation of its optical gain with increasing temperature, which is indicated by the greater increase of the threshold current density at high temperatures. As a result, an increase in the maximum operating temperature of only 1 K is observed for the Ag-based device B2, which is smaller than the 5-K increase observed for (Ag-based) B1. The output power of the Ag-based device is 20% higher for B1 and 30% higher for B2, with the improvement in the quantum efficiency a little smaller for B2.

Figure 8 shows the THz-power-current-voltage (LIV) characteristics and the emission spectra of the two QCLs from the wafer A2. The I-V curves and the emission spectra of the two devices are similar, indicating that the Ag waveguide has only a small influence on the electrical conduction and the net gain spectra. The emission of both the Ag- and Au-based devices is centered at ~ 3.4 THz, a little higher than the frequency of 3.1 THz used in the modeling. This could contribute to the overestimation of the maximum operating temperature discussed above. Compared with Au, Ag is more chemically reactive, potentially leading to oxidation issues during device processing. We

found that a Au protection film deposited on the top of the Ag layer is quite effective to reduce these effects. Additionally, omitting the oxygen-plasma cleaning process also helps. Nevertheless, the I-V curves show a higher terminal voltage for Ag-based devices, compared with Au-based devices, which can be attributed to oxidation of Ag waveguide layers during the device fabrication. The same device was characterised after it had been placed in air for more than two years, and the results are shown in Fig. 8. The threshold current becomes a little larger, from 860 A/cm^2 to 875 A/cm^2, and the output power is a little lower. However, the I-V curves and the maximum operating temperature remain almost unchanged.

5. Discussions and conclusions

Several further areas for investigation of Ag waveguides have been identified. Firstly, the higher thermal conductivity of the Ag film, compared to the Au film, can also contribute to the increase in the operating temperature. This contribution is more important for the double metal waveguide than the surface plasmon waveguide, and need to be investigated especially for the devices operating in CW mode. Secondly, the Ag film was found to oxidize in the air during the device processing, even though it was capped with a Au film. The effects of this oxidation on the device performance and potential protection methods are worthy of further investigation. Thirdly, the quality and the thickness of the Ag film could affect its resistivity. Compared to the Au film, 50 nm thicker Ag and Cu films were used for the resistivity measurement and waveguide fabrication, with the purpose of reducing the effects of oxidation. However, the surface scattering and grain boundary scattering could be reduced, and this could lead to an overestimation of the advantages of Ag-based waveguides. The effect of the deposition methods and the film thickness on the waveguide properties need to be addressed, and further investigations of the electron density, impurities and scattering properties of the thin Ag film are needed for improved modeling. Finally, our simulations suggest that there would be an improvement using Ag layers in DM waveguides. It is of interest to investigate experimentally the use of Ag-based DM waveguides, which will be helpful for the future development of THz QCLs operating at high temperatures.

In conclusion, the dielectric constants of Ag, Au and Cu films were calculated based on the Drude model, in which the damping frequencies were extracted from the measured dc resistivity. The waveguide analysis showed that Ag-based devices exhibit superior performance to equivalent Au- and Cu-based devices, with the magnitude of the improvements being dependent on the active-region design. The adhesion layer and the top contact layer have similar effects on the waveguide performance, and lead to small variations of the threshold gain. Good agreement was found between the waveguide analysis and the experimental characteristics of Ag- and Au-based devices. Compared with Au-based devices, improvements of 5-13 K in the maximum operating temperature were observed except for the wafer B2. This exceeds the typical ~ 2 K variation in devices obtained from a given wafer. As such, we conclude that Ag waveguides can potentially yield an improvement in high-temperature performance compared with Au or Cu waveguides..

Funding

The Engineering and Physical Sciences Research Council (EPSRC) (EP/J017671/1 and EP/P021859/1); Royal Society and Wolfson Foundation (WM110032, WM150029); UK Centre for Earth Observation Instrumentation (RP10G0435A03) and European Space Agency (4000114487/15/NL/AF).

Acknowledgments

The data associated with this paper are openly available from the University of Leeds data repository. https://doi.org/10.5518/241.